

Atmospheric Correction of Satellite Ocean Color Imagery: The Black Pixel Assumption

David A. Siegel^{1,2}, Menghua Wang³,
Stéphane Maritorena¹ and Wayne Robinson⁴

¹Institute for Computational Earth System Science, University of California, Santa Barbara,
Santa Barbara, CA, 93106-3060, U.S.A.

²Also, Department of Geography and Donald Bren School of Environmental Science and Management, University of California, Santa Barbara

³University of Maryland Baltimore County, NASA Goddard Space Flight Center, Greenbelt, MD

⁴SAIC General Sciences Corporation, NASA Goddard Space Flight Center, Greenbelt, MD

Submitted to *Applied Optics*, September 10, 1999

Resubmitted: May 3, 2000

Acknowledgments

Bob Arnone and Rick Stumpf brought the issue of the black pixel assumption to our attention and their encouragement through this process is appreciated. Discussions and encouragement from Chuck McClain, Howard Gordon and André Morel are gratefully acknowledged as are the detailed comments from the anonymous reviewers. We thank Andrea Magnuson and Larry Harding for providing SeaWiFS imagery and field data from Chesapeake Bay and Brian Schieber for the SIMBIOS matchup data. The authors gratefully acknowledge the support of NASA as part of the SIMBIOS and SeaWiFS science teams. The U.S. EPA and the state governments bordering Chesapeake Bay supported chlorophyll observations presented. The SeaWiFS satellite mission is a joint venture of the Orbital Sciences Corporation and NASA.

ABSTRACT

The assumption that values of water leaving radiance in the near-infrared (NIR) are negligible enable aerosol radiative properties to be easily determined in the correction of satellite ocean color imagery. This is referred to as the black pixel assumption. We examine the implications of the black pixel assumption using a simple bio-optical model for the NIR water-leaving reflectance, $[\rho_w(\lambda_{NIR})]_N$. In productive waters (chlorophyll [*Chl*] concentration $> 2 \text{ mg m}^{-3}$), estimates of $[\rho_w(\lambda_{NIR})]_N$ are several orders of magnitude larger than those expected for pure seawater. These large values of $[\rho_w(\lambda_{NIR})]_N$ result in an over correction of atmospheric effects for retrievals of water-leaving reflectance which are most pronounced in the violet and blue spectral region. The over correction increases dramatically with *Chl* reducing the true water-leaving radiance by roughly 75% when *Chl* is equal to 5 mg m^{-3} . Relaxing the black pixel assumption in the correction of Sea-viewing Wide-Field of view Sensor (SeaWiFS) satellite ocean color imagery provides significant improvements in *Chl* and water-leaving reflectance retrievals when *Chl* values are greater than 2 mg m^{-3} . Improvements in the present modeling of $[\rho_w(\lambda_{NIR})]_N$ are considered, particularly for turbid coastal waters. However, this work shows that the effects of non-zero NIR reflectance must be included in the correction of satellite ocean color imagery.

1. Introduction

It is well recognized that more than 90% of the signal measured by an ocean color satellite sensor is due to the confounding influence of the atmosphere. The atmospheric and ocean surface effects must be removed before ocean radiance signals may be analyzed for the purposes of understanding the ocean biosphere. This step in the processing of satellite ocean color imagery is referred to as the atmospheric correction procedure.¹ Typically, the satellite sensed radiance, $L_t(\lambda)$, or equivalently reflectance, $\rho_t(\lambda)$ ($= \pi L_t(\lambda)/(F_o(\lambda)\mu_o$) where $F_o(\lambda)$ is the extraterrestrial solar irradiance and μ_o is the cosine of the solar zenith angle), is partitioned into components corresponding to distinct physical processes, or

$$\rho_t(\lambda) = \rho_r(\lambda) + \rho_a(\lambda) + \rho_{ra}(\lambda) + T(\lambda)\rho_g(\lambda) + t(\lambda)\rho_{wc}(\lambda) + t(\lambda)\rho_w(\lambda). \quad (1)$$

The first three terms on the right-hand side of equation (1) represent the contributions from atmospheric scattering due to air molecules (Rayleigh), aerosols, and Rayleigh-aerosol interactions, respectively. The terms $T(\lambda)$ and $t(\lambda)$ are the direct and diffuse transmittances of the atmospheric column, respectively, $\rho_g(\lambda)$ represents the effects of sun glitter off the sea surface, $\rho_{wc}(\lambda)$ is the reflectance of ocean whitecaps and $\rho_w(\lambda)$ is the water-leaving reflectance, the desired quantity in ocean color remote sensing.^{1,2} In equation (1), the Rayleigh scattering term, $\rho_r(\lambda)$, and transmittances, $T(\lambda)$ and $t(\lambda)$, can be accurately calculated,^{3,4,5,6} the ocean whitecap contributions can be estimated using the surface wind speed,^{7,8,9} and sun glitter contaminated observations are generally avoided. This leaves the contributions from scattering by aerosols and Rayleigh-aerosol interactions, $\rho_a(\lambda) + \rho_{ra}(\lambda)$, and the ocean, $\rho_w(\lambda)$, as unknowns to be determined. To solve for these terms, it is first assumed that the NIR water leaving radiance is negligible enabling estimates of NIR aerosol scattering terms to be made. Values of $\rho_a(\lambda) + \rho_{ra}(\lambda)$ for the visible bands are arrived at by extrapolating the near-infrared aerosol signals into the visible using appropriate aerosol models.² The assumption that the NIR ocean is opti-

cally black ($\rho_w(\lambda_{NIR}) = 0$) was initially made for clear ocean waters¹⁰ and is referred to as the black pixel assumption.

To relate the derived water-leaving reflectance to the inherent optical properties of the ocean, all geometric influences on $\rho_w(\lambda)$ must be eliminated. This is done by normalizing the water-leaving reflectance, $[\rho_w(\lambda)]_N$, to a zenith sky similar to the definition of the normalized water-leaving radiance, $[L_w(\lambda)]_N$,¹⁰

$$[L_w(\lambda)]_N = L_w(\lambda) / \mu_0 t_0(\lambda) \quad (2)$$

and

$$[\rho_w(\lambda)]_N = \frac{\pi [L_w(\lambda)]_N}{F_0(\lambda)} = \frac{\rho_w(\lambda)}{t_0(\lambda)}, \quad (3)$$

where $t_0(\lambda)$ is the atmospheric diffuse transmittance in the solar direction. Ocean constituent concentrations are determined from estimates of $[\rho_w(\lambda)]_N$ using either empirical^{11,12} or semi-analytical^{13,14,15} models.

The Sea-viewing Wide Field-of-view Sensor (SeaWiFS) has provided the oceanographic community an unprecedented opportunity to assess globally ocean biological and biogeochemical processes.¹⁶ SeaWiFS imagery are available with a spatial resolution of 1.1 km (at nadir) and a sampling schedule of nearly once per day. The SeaWiFS atmospheric correction procedure assumes that bands 7 and 8 (centered at 765 and 865 nm, respectively) are “black pixels” and are used to estimate aerosol radiance levels and to select appropriate aerosol optical models.² For the open ocean conditions, the atmospheric correction algorithm is thought to be accurate to within 5%.²

Unfortunately, the SeaWiFS determinations of water leaving reflectance in the violet and blue (SeaWiFS bands 1 and 2) underestimate dramatically in situ observations for highly productive waters (i.e., low $[\rho_w(\lambda)]_N$ retrievals). This can be seen in a comparison of nearly simultaneous match-ups of SeaWiFS and field observations of $[\rho_w(\lambda)]_N$ at 412,

443 and 490 nm and chlorophyll (*Chl*) concentration (figure 1) provided from the Sensor Intercomparison and Merger for Biological and Interdisciplinary Oceanic Studies (SIMBIOS) project. Details of the procedures used in developing these satellite-field data comparisons may be found in Ref. 17. Obviously, the present version of SeaWiFS processing (version 2) underestimates determinations of $[\rho_w(412)]_N$ when values of $[\rho_w(412)]_N$ are small (less than 0.005; figure 1a). A similar, though less pronounced, underestimation is found for $[\rho_w(443)]_N$ (figure 1b). However, the comparison of the field and satellite *Chl* is good with no real bias from the one-to-one line (figure 1d). In general, SeaWiFS provides excellent *Chl* retrievals explaining 81% of the observed variance.

Several factors may be responsible for poor performance of the SeaWiFS atmospheric correction procedure. However, the over-correction for $[\rho_w(\lambda)]_N$ retrievals is most apparent for low values of $[\rho_w(412)]_N$ when *Chl* observations are large. This suggests that this problem may be due to the ocean itself. We hypothesize that the inappropriate application of the black pixel assumption is responsible for some of the problems highlighted in Figure 1. This was first suggested by Robert Arnone and his colleagues¹⁸ and other researchers have worked on this issue as well.^{19,20} Here, we study the implications of the black pixel assumption on the correction of satellite ocean color imagery. First, we develop a simple bio-optical algorithm for estimating $[\rho_w(\lambda_{NIR})]_N$ and quantify its magnitude using a recent ocean optics climatology.¹² We evaluate theoretically the implications of relaxing the black pixel assumption on estimates of water-leaving radiance and provide an iterative correction scheme. Last, we will demonstrate the implications of the black pixel assumption using SeaWiFS imagery.

2. Estimation of Ocean Contributions at the NIR Bands

Measurements of the water-leaving radiance spectrum have now become routine because of the need to calibrate and validate satellite ocean color imagery. However, to the best of our knowledge, no direct estimates of $[\rho_w(\lambda_{NIR})]_N$ are available due to extreme dif-

difficulty in making upwelling NIR radiance measurements. Hence, values for $[\rho_w(\lambda_{NIR})]_N$ are most expediently estimated using optical models and knowledge of NIR inherent optical properties.

Values of $[\rho_w(\lambda)]_N$ can be modeled as a function of the spectral absorption ($a(\lambda)$) and backscattering ($b_b(\lambda)$) coefficients,¹³ or

$$[\rho_w(\lambda)]_N = (t/n)^2 \prod_{i=1}^2 g_i \frac{b_b(\lambda)}{b_b(\lambda) + a(\lambda)} \quad (4)$$

where $(t/n)^2$ accounts for the transmission of upwelling radiance and downwelling irradiance across the sea surface²¹ and the constants g_1 and g_2 are 0.0949 sr^{-1} and 0.0794 sr^{-1} , respectively.¹³

Absorption of NIR radiation by seawater dominates over other factors enabling $a(\lambda_{NIR})$ to be modeled using its pure water value, $a_w(\lambda_{NIR})$.^{22,23} For the case where bands in the red spectral region are required for atmospheric correction scheme, an accounting of particulate-induced absorption is required.²⁴ On the other hand, the modeling of the backscattering coefficient is problematic as values of $b_b(\lambda_{NIR})$ due to particulates are much larger than those due to seawater.^{15,25} Hence, a predictive knowledge of the particulate backscattering coefficient, $b_{bp}(\lambda_{NIR})$, is required. Provided a model for $b_{bp}(\lambda_{NIR})$, estimates of NIR normalized water-leaving reflectance may be expressed as

$$[\rho_w(\lambda_{NIR})]_N = (t/n)^2 \prod_{i=1}^2 g_i \frac{b_{bp}(\lambda_{NIR}) + b_{bw}(\lambda_{NIR})}{b_{bp}(\lambda_{NIR}) + b_{bw}(\lambda_{NIR}) + a_w(\lambda_{NIR})} \quad (5)$$

where the necessary parameters are presented in Table 1.

We compare two basic approaches for determining $b_{bp}(\lambda_{NIR})$. The first uses estimates of the chlorophyll *a* concentration to determine $b_{bp}(\lambda_{NIR})$ ^{11,26} while the second uses determinations of water leaving radiance and the assumption of optical closure.¹⁵ Both rela-

tionships are empirical and were derived from field data within the visible spectral region and extrapolated into the NIR.

The bio-optical modeling of $b_{bp}(\lambda_{NIR})$ assumes that its variability is driven by the chlorophyll content of the water, or

$$b_{bpBO}(\lambda_{NIR}) = 0.416 Chl^{0.766} \left(0.002 + (550/\lambda_{NIR}) (0.02 (0.5 - 0.25 \log_{10}(Chl))) \right) \quad (6)$$

where Chl is the chlorophyll concentration (in mg m^{-3}) and λ_{NIR} is the center NIR wavelength of interest. The term outside of the parentheses on the right hand side of equation 6 gives the particulate scattering coefficient at 550 as recently updated²⁷ while the term within parentheses models the spectral dependence and the magnitude of the backscattered fraction. This formulation assumes that the spectral dependence for $b_{bpBO}(\lambda_{NIR})$ goes as λ^{-1} throughout the entire spectral range. Similar bio-optical algorithms are available^{13,26} all of which give broadly similar results (within a factor of 4 for $[\rho_w(\lambda_{NIR})]_N$; comparison not shown).

The optical closure backscatter model, $b_{bpOC}(\lambda_{NIR})$, is derived from reflectance-based estimates of $b_{bp}(\lambda)$.¹⁵ This parameterization assumes that the magnitude of spectral backscatter is a linear function of the water-leaving reflectance at 551 nm, $[\rho_w(551)]_N$, while the spectral slope of particulate backscatter is a function of the ratio of $[\rho_w(443)]_N$ to $[\rho_w(488)]_N$, or

$$b_{bpOC}(\lambda_{NIR}) = \left(X_0 + X_1 [\rho_w(551)]_N \right) \frac{551^{Y_0 + Y_1 [\rho_w(443)]_N / [\rho_w(488)]_N}}{\lambda_{NIR}} \quad (7)$$

where $X_0 = -0.00182$, $X_1 = 0.655$, $Y_0 = -1.13$, and $Y_1 = 2.57$.¹⁵ The ratio of $[\rho_w(443)]_N$ to $[\rho_w(488)]_N$ is large in blue waters and small in green and turbid waters causing the spectral slope for $b_{bpOC}(\lambda_{NIR})$ to vary from 0 for turbid waters to greater than 2 for clear, oligotrophic waters. The magnitude of $b_{bpOC}(\lambda_{NIR})$ is controlled by $[\rho_w(551)]_N$ where, to first order, backscattering regulates ocean color variability.¹¹

The two estimates of $b_{bp}(\lambda)$ are plotted against Chl in figure 2a for $b_{bp}(550)$ and in figure 2b for $b_{bp}(865)$ for the SeaBAM data set.¹² Values of $b_{bp}(550)$ are comparable to the pure water values (the dotted line in figure 2a) whereas estimates of $b_{bp}(865)$ are often a factor of 10 greater than $b_{pw}(865)$. Compared with the bio-optical determinations of $b_{bp}(550)$ and $b_{bp}(865)$, the closure-based estimates are a weaker function of Chl , particularly at 550 nm. Mean values of $b_{bp}(550)$, $b_{bp}(760)$ and $b_{bp}(865)$ are similar for both methods (Table 2).

Scale estimates for $[\rho_w(\lambda_{NIR})]_N$ can be made using both methods for determining $b_{bp}(\lambda_{NIR})$ (figures 2c and 2d). As expected, an increasing trend in $[\rho_w(\lambda_{NIR})]_N$ is found with increasing Chl where values of $[\rho_w(865)]_N$ increase from 10^{-5} for $Chl = 0.5 \text{ mg m}^{-3}$ to nearly 10^{-3} for $Chl > 10 \text{ mg m}^{-3}$. Both estimates of $[\rho_w(\lambda_{NIR})]_N$ are much greater than expected for pure seawater (where $b_{bp}(\lambda_{NIR}) = 0$ and $a(\lambda_{NIR}) = a_w(\lambda_{NIR})$; the dotted line in figures 2c and 2d). Estimates of $[\rho_w(\lambda_{NIR})]_N$ found using the bio-optical $b_{bp}(\lambda)$ algorithm are similar to the optical closure model although large degree of scatter is observed among these estimates of $[\rho_w(\lambda_{NIR})]_N$ (fig. 2c and d; Table 3).

The importance of the black pixel assumption to SeaWiFS imagery can be evaluated by comparing the present estimates of $[\rho_w(\lambda_{NIR})]_N$ to the single digital count (DC) sensed by the SeaWiFS instrument.²⁸ Estimates of $[\rho_w(\lambda_{NIR})]_N$ are greater than the SeaWiFS 1 DC level (the dashed lines in figures 2c and 2d) for $Chl > \sim 0.5 \text{ mg m}^{-3}$. Hence, NIR water-leaving radiance may be important for the atmospheric correction of SeaWiFS imagery in moderate to highly productive waters.

The choice of the appropriate $[\rho_w(\lambda_{NIR})]_N$ parameterization is not straightforward as there are few direct observations of backscatter that may be used to develop or validate a parameterization. The bio-optical approach has been applied extensively within the ocean optics community^{11,24,26} whereas the closure model has been recently introduced and has not been independently validated.¹⁵ Both $b_{bp}(\lambda_{NIR})$ models have extensive uncertainties which feed into the modeling of $[\rho_w(\lambda_{NIR})]_N$. For present purposes, we will use the bio-

optical approach simply because it is the "known quantity" of the two candidates. It is likely that future implementations of a black pixel correction procedure will use approaches similar to the closure model, especially for turbid, coastal and inland waters (see section 5 for further discussion).

3. Effects of the Black Pixel Assumption on the SeaWiFS Atmospheric Correction Algorithm

3A. Errors in $[\rho_w(\lambda)]_N$ Retrievals

We address the importance of the black pixel assumption and its effect on $[\rho_w(\lambda)]_N$ retrievals using the present version of the SeaWiFS atmospheric correction algorithm² with a maritime aerosol model, a relative humidity (RH) of 80% (M80) and an aerosol optical thickness at 865 nm of 0.1. We compare retrievals using a fully black ocean ($[\rho_w(\lambda)]_N = 0$ for all λ) to those made for an ocean that is black in the visible ($[\rho_w(\lambda)]_N = 0$ for $400 < \lambda < 700$ nm) but which reflectance in the NIR, $[\rho_w(\lambda_{NIR})]_N$, is a known function of *Chl* (given by equations 5 and 6). The assumed water-leaving signals are used in the calculation of the top-of-the-atmosphere (TOA) reflectance spectra from which $[\rho_w(\lambda)]_N$ are then computed and corrected for inherent noise (≈ 0.001 in reflectance units^{1,2,29}). The difference between retrieved $[\rho_w(\lambda)]_N$ for the fully black ocean and for the non-zero NIR ocean, $[\rho_w(\lambda)]_N$, quantifies the importance of the black pixel assumption.

Estimates of $[\rho_w(\lambda)]_N$ illustrate the effects of varying NIR water reflectance on retrievals of $[\rho_w(\lambda)]_N$ (Fig 3). In these depictions, two solar and viewing geometries ($\theta_0 = 20^\circ$, $\theta = 20^\circ$, $\phi = 90^\circ$; figure 3a and 3c and $\theta_0 = 40^\circ$, $\theta = 40^\circ$, $\phi = 90^\circ$; figure 3b and 3d) are shown. The magnitude of the error term, $[\rho_w(\lambda)]_N$, is shown in figures 3a and 3b and normalized error estimates are given in figures 3c and 3d where the bio-optical model of Ref. 13 is employed. Similar results were obtained for other aerosol

models, aerosol optical thicknesses, and solar and viewing geometry (results not shown).

In general, values of $[\rho_w(\lambda)]_N$ increase dramatically with Chl and this effect is more accentuated for the blue wavebands (Fig 3). Ignoring the NIR ocean contributions leads to an overcorrection of aerosol reflectance. The effects become important ($>10\%$ of the retrieved $[\rho_w(\lambda)]_N$) for $Chl > 0.5 \text{ mg m}^{-3}$. Hence, for oligotrophic conditions, existing SeaWiFS correction algorithms should perform well. However, errors will be large for ocean regions with high chlorophyll concentrations.

3B. Errors in Two-Band Ratio Chlorophyll Retrievals

Many algorithms for determining ocean chlorophyll concentrations use ratios of normalized water-leaving reflectance.^{11,12} For example, the OC2v2 chlorophyll algorithm uses the ratio of SeaWiFS bands 3 and 5 ($R(3,5) = [\rho_w(490)]_N / [\rho_w(555)]_N$) in a polynomial relationship.³⁰ We quantify the error due to the black pixel assumption for any arbitrary band ratio, $R(i, j)$, as

$$R(i, j) = \frac{[\rho_w(\lambda_i)]_N + [\rho_w(\lambda_i)]_N}{[\rho_w(\lambda_j)]_N + [\rho_w(\lambda_j)]_N} - \frac{[\rho_w(\lambda_i)]_N}{[\rho_w(\lambda_j)]_N} \quad (8)$$

where i and j are the SeaWiFS band numbers. Determinations of $R(i, j)$ are made using the previous calculations of $[\rho_w(\lambda)]_N$ and values of $[\rho_w(\lambda)]_N$ estimated from the semi-analytical algorithm of Ref. 13. Typical errors in the retrieved ratio values between SeaWiFS bands 2 and 5, $R(2,5)$, and bands 3 and 5, $R(3,5)$, are shown in Table 4. As before, the M80 aerosol model with aerosol optical thickness of 0.1 at 865 nm and the two solar and viewing geometries are used. The present results show that for Chl less than 1 mg m^{-3} , differences due to the application of a NIR correction are small ($\sim 2\%$). However for Chl greater than 2 mg m^{-3} , band ratio errors increase dramatically (Table 4). Errors are greater than 20% for $R(3,5)$ and more than 60% for $R(2,5)$ for a Chl of 5 mg m^{-3} . Band ratio errors are greater for $R(2,5)$ than for $R(3,5)$ as expected.

We compare the effects of the black pixel assumption using the present version of

the SeaWiFS algorithm and a polynomial band ratio algorithm using $R(2, 5)$ (Morel-3 algorithm in Ref. 12). For low Chl waters ($Chl < 0.5 \text{ mg m}^{-3}$), the errors in chlorophyll retrievals are not large ($< 5\%$; Table 5). However for $Chl > 2 \text{ mg m}^{-3}$, the errors can be greater than 100%. For high Chl conditions, the errors due to the NIR ocean contribution are greater for the Morel-3 algorithm than for the OC2v2 algorithm as Morel-3 relationship uses the $R(2,5)$ ratio (Table 5). We conclude that the NIR ocean contribution must be included in the atmospheric correction schemes for moderate to high Chl conditions.

3C. Accounting for $[\rho_w(\lambda_{NIR})]_N$ in the SeaWiFS Atmospheric Correction Procedure

The accounting of $[\rho_w(\lambda_{NIR})]_N$ in atmospheric correction requires an iterative approach. The iterative procedure entails an initial guess for Chl , an estimate for $[\rho_w(\lambda_{NIR})]_N$ and its removal from the reflectance budget (equation 1), and application of the existing SeaWiFS atmospheric correction algorithm to retrieve a new Chl . This process is repeated until a converged Chl value is obtained. The NIR correction procedure can be summarized schematically as follows:

$$\underbrace{Chl_0}_{\text{Initial}} \quad \underbrace{[\rho_w(\lambda_{NIR})]_N \quad \text{Atmos. Corr.} \quad [\rho_w(\lambda)]_N \quad \& \quad Chl \quad \text{repeat}}_{\text{Iterations}} \quad (10)$$

The initial Chl value, Chl_0 , is set to 0.2 mg m^{-3} and iterations are stopped once the final Chl retrieval is within 20% of the last iterate. Typically, 1 (open ocean) to 3 (coastal waters) iterations are required. If the first iterated Chl value is less than 0.3 mg m^{-3} , the iterations are terminated.

4. Application to SeaWiFS imagery

To assess the importance of the black pixel assumption, we apply the NIR correction scheme to SeaWiFS imagery on both local and global scales. First, we use a SeaWiFS local area coverage (LAC) image from the Chesapeake Bay region demonstrating that misapplication of the black pixel assumption leads to large errors in highly productive wa-

ters. Next, we assess changes in the SIMBIOS global field-satellite match-up data set after correcting for $[\rho_w(\lambda_{NIR})]_N$. Last, we evaluate the effects of the black pixel assumption on global SeaWiFS imagery.

4A. An Example of SeaWiFS Imagery from Chesapeake Bay

As discussed previously, SeaWiFS chlorophyll retrievals often overestimate *Chl* values in productive waters (figure 1). A SeaWiFS LAC *Chl* image from May 19, 1998 for the Chesapeake Bay region (east coast of North America) is shown in figure 4a. Using the standard processing, most of the *Chl* retrievals throughout the bay are in excess of 64 mg m^{-3} which is the maximum value quantified (figure 5a). However, no field observations from this period show values in excess of 40 mg m^{-3} (figure 5c). A re-analysis of this SeaWiFS image using the present NIR parameterization shows substantial improvements (figure 4b). In particular, nearly all of the excessive *Chl* retrievals ($> 40 \text{ mg m}^{-3}$) have been corrected and the range of *Chl* retrievals is now consistent with the field observations (figure 5b and 5c).

4B. Global *in situ* match-up analyses

Despite the limited number of observations at high chlorophyll concentration, the global matchup data set reprocessed with the present NIR algorithm shows improvements compared with the original analysis (figure 6). In particular, the regression slope between the two $[\rho_w(412)]_N$ retrievals is closer to one for the NIR corrected data. Similarly, root mean square (rms) deviations between the satellite and field observations are significantly less for the NIR processed SeaWiFS retrievals for $[\rho_w(\lambda)]_N$ and *Chl* (figure 6).

Consistent with what is seen with the example from Chesapeake Bay (figures 4 and 5), there is a significant improvement in the correspondence between the SeaWiFS and field estimates of *Chl* at high concentrations (figure 7). For $Chl > 1 \text{ mg m}^{-3}$, rms differences in *Chl* retrievals are smaller for the NIR processing (1.46 mg m^{-3}) than with the

standard processing (2.04 mg m^{-3}).

4C. Global Imagery Analysis

Analysis of global imagery enables the importance of the NIR correction to be put in context. Figure 8 shows frequency of occurrence distributions of the NIR error from two SeaWiFS *Chl* 8-day composite scenes (summer, Jul. 12 - 19, 1998, and winter, Jan. 17 - 24, 1998). The effects of the bio-optical NIR algorithm on global *Chl* retrievals is only important ($> 10\%$) when the standard processing *Chl* is greater than 2 mg m^{-3} . These conditions occur for only 2.1 and 1.3% of total number of good retrievals for the summer and winter composites, respectively. However, the effects of NIR water-leaving reflectance reach nearly 60% of the standard processing value (figure 8). The small ($<10\%$) normalized *Chl* errors found for $Chl < 0.02 \text{ mg m}^{-3}$ are due to the amplification of small round-off errors (which are order 0.001 mg m^{-3}) by the small normalization factor.

The role of the black pixel assumption on retrievals of water-leaving reflectance can also be addressed (figure 9). As seen before, only for the highest *Chl* categories shown will the misapplication of the black pixel assumption have a large influence ($> 20\%$) on the retrieved $[\rho_w(\lambda)]_N$ spectrum (figure 9). Significant effects ($\sim 10\%$) are also observed for the 1-2 mg m^{-3} category. Hence, NIR water-leaving reflectance must be considered in the global processing of ocean color imagery.

5. Discussion and Future Directions

The present study demonstrates that the black pixel assumption in ocean color remote sensing must be considered where *Chl* is greater than 2 mg m^{-3} . For these waters, the shape of the retrieved water-leaving reflectance spectrum is strongly altered and *Chl* retrievals will be overestimated if the NIR water-leaving signal is not accounted for. However, several aspects of the NIR correction procedure are not well understood. These include the assumptions used to relate the NIR water-leaving reflectance to NIR

inherent optical properties and the modeling of NIR inherent optical properties as a function of *Chl*. In the following, we address these issues and provide some thoughts about future research directions.

Many important radiative transfer processes have been neglected in the present estimates of $[\rho_w(\lambda_{NIR})]_N$. These include the contributions to the water-leaving radiance due to Raman scattering, inconsistency with the bidirectional reflectance distribution function (BRDF) for NIR wavebands and the influence of changes in the ambient ocean temperature on the present determinations of $[\rho_w(\lambda_{NIR})]_N$. These issues may be addressed using a radiative transfer model (Hydrolight vers. 4.02³¹). The inclusion of Raman scattering processes should increase the NIR water-leaving reflectance, $[\rho_w(\lambda_{NIR})]_N$. We find that for *Chl* greater than $\sim 0.5 \text{ mg m}^{-3}$ and reasonable solar zenith angles, the error of not including Raman scattering in estimating $[\rho_w(\lambda_{NIR})]_N$ is less than 5% (results not shown). Only for oligotrophic concentrations ($Chl = 0.05 \text{ mg m}^{-3}$), do errors approach 10%. Hence, Raman scattering is not important to the modeling of $[\rho_w(\lambda_{NIR})]_N$.

Another poorly constrained factor is the BRDF. We evaluated differences in water-leaving radiance in the plane perpendicular to the solar plane for wavelengths of 443 and 765 nm under different solar illumination geometries and *Chl* concentrations. The anti-solar plane is used to represent the scan line sampled by an ocean color imager. We find differences in the water-leaving radiance along the scan line normalized to the nadir looking radiance estimate are consistent between the 443 and 765 nm wavebands (within 10% in the worst case). Further, no large differences are found with changes in solar zenith angle or *Chl*. Hence, BRDF changes are similar for the NIR wavebands as they are in the visible wavebands and this is likely to be a minor issue in determining $[\rho_w(\lambda_{NIR})]_N$.

Changes in ambient seawater temperature can also affect estimates of $[\rho_w(\lambda_{NIR})]_N$ by altering the absorption coefficient for seawater. Values of $a_w(750)$ change with increasing temperature by the factor $0.0106 \text{ m}^{-1} \text{ }^\circ\text{C}^{-1}$.³² Assuming clear water conditions ($Chl = 0$), a 4% decrease in the value of $[\rho_w(750)]_N$ is expected for a 10 $^\circ\text{C}$ increase of seawater

temperature. Hence, temperature-induced changes in seawater inherent optical properties should not have a significant effect on NIR correction procedures.

The present NIR correction procedure provides significant improvements in SeaWiFS retrievals especially for productive waters. However, the modeling of $b_{bp}(\lambda_{NIR})$ as a function of *Chl* is an important limitation. This parameterization is reasonable for Case I waters where phytoplankton regulate the inherent optical properties of the ocean. However, it is questionable for turbid, coastal waters (Case II oceans) where backscatter can originate from constituents other than phytoplankton.^{25,33} These materials include detrital biological material and abiotic particulates such as suspended sediments. For that reason, the modeling of $b_{bp}(\lambda_{NIR})$ on a closure-based basis, such as given in equation (7), is likely to be the long term solution. The implementation of this approach requires an accurate development data set and, to the best of our knowledge, these data currently do not exist.

Clearly, there are limits on the validity of the black pixel assumption. A value of *Chl* of 2 mg m^{-3} appears to be a good breakpoint above which NIR effects must be considered. However, the misapplication of the black pixel assumption is not the only factor causing the over correction of SeaWiFS water-leaving radiance spectra in the violet and blue region. More research into improving our ability to correct ocean color imagery is required.

REFERENCES

1. H.R. Gordon, "Atmospheric correction of ocean color imagery in the Earth Observing System era," *J. Geophys. Res.* **102**, 17,081-17,106 (1997).
2. H.R. Gordon & M. Wang, "Retrieval of water-leaving radiance and aerosol optical thickness over the oceans with SeaWiFS: A preliminary algorithm," *Appl. Opt.* **33**, 443-452 (1994).
3. H.R. Gordon, J.W. Brown, & R.H. Evans, "Exact Rayleigh scattering calculations for use with the Nimbus-7 Coastal Zone Color Scanner," *Appl. Opt.* **27**, 862-871 (1988).
4. H.R. Gordon, & M. Wang, "Surface roughness considerations for atmospheric correction of ocean color sensors. 1: The Rayleigh scattering component," *Appl. Opt.*, **31**, 4,247-4,260 (1992).
5. M. Wang, "Atmospheric correction of ocean color sensors: Computing atmospheric diffuse transmittance," *Appl. Opt.* **38**, 451-455 (1999).
6. H. Yang, & H.R. Gordon, "Remote sensing of ocean color: assessment of water-leaving radiance bidirectional effects on atmospheric diffuse transmittance," *Appl. Opt.* **36**, 7,887-7,897 (1997).
7. H.R. Gordon, & M. Wang, "Influence of oceanic whitecaps on atmospheric correction of ocean-color sensor," *Appl. Opt.* **33**, 7,754-7,763 (1994).
8. R. Frouin, M. Schwindling, & P.Y. Deschamps, "Spectral reflectance of sea foam in the visible and near-infrared – In situ measurements and remote sensing implications," *J. Geophys. Res.* **101**, 14,361-14,371 (1996).
9. Moore, K.D., K.J. Voss, & H.R. Gordon, "Spectral reflectance of whitecaps: Their contribution to water-leaving radiance," *J. Geophys. Res.*, **105**, 6493-6499 (2000).

10. H.R. Gordon, & D.K Clark, "Clear water radiances for atmospheric correction of coastal zone color scanner imagery," *Appl. Opt.* **20**, 4,175-4,180 (1981).
11. H.R. Gordon, & A.Y. Morel, "Remote Assessment of Ocean Color for Interpretation of Satellite Visible Imagery: A Review," Springer-Verlag, New York, 114 pp. (1983).
12. J.E. O'Reilly, S. Maritorena, B.G. Mitchell, D.A. Siegel, K.L. Carder, S.A. Garver, M. Kahru, & C.R. McClain, "Ocean color chlorophyll algorithms for SeaWiFS," *J. Geophys. Res.* **103**, 24,937-24,953 (1998).
13. H.R. Gordon, O.B. Brown, R.H. Evans, J.W. Brown, R.C. Smith, K.S. Baker, & D.K. Clark, "A semianalytic radiance model of ocean color," *J. Geophys. Res.* **93**, 10,909-10,924 (1988).
14. S.A. Garver, & D.A. Siegel, "Inherent optical property inversion of ocean color spectra and its biogeochemical interpretation: I. Time series from the Sargasso Sea," *J. Geophys. Res.* **102**, 18,607-18,625 (1997).
15. K.L. Carder, F.R. Chen, Z.P. Lee, S.K. Hawes, & D. Kamykowski, "Semianalytic Moderate-Resolution Imaging Spectrometer algorithms for chlorophyll a and absorption with bio-optical domains based on nitrate-depletion temperatures," *J. Geophys. Res.* **104**, 5,403-5,421 (1999).
16. C.R. McClain, M.L. Cleave, G.C. Feldman, W.W. Gregg, S.B. Hooker, & N. Kuring, "Science Quality SeaWiFS Data for Global Biosphere Research," *Sea Technology*, 10-16 (1998).
17. B.D. Schieber, & C.R. McClain, " L_{wN} and chlorophyll-a matchup analyses," SeaWiFS Postlaunch Technical Report Series, NASA Tech. Memo. 1999-206892, S.B. Hooker and E.R. Firestone, Eds., NASA Goddard Space Flight Center, Greenbelt, Maryland, (accepted) (2000).

18. R.A. Arnone, P. Martinolich, R.W. Gould, M. Sydor, R.P. Stumpf, "Coastal optical properties using SeaWiFS", Presented at Ocean Optics XIV, Kailua-Kona, HI, November 10-13, 1998, (1998).
19. Ruddick, KG; Ovidio, F; Rijkeboer, M. Atmospheric correction of SeaWiFS imagery for turbid coastal and inland waters. *APPLIED OPTICS*, FEB 20, 2000, V39(N6):897-912.
20. Hu, C., K.L. Carder, and F. Muller-Karger (2000), Atmospheric correction of SeaWiFS imagery over turbid coastal waters: a practical method, *Remote Sens. Environ.* (in press).
21. R.W. Austin, "The remote sensing of spectral radiance from below the ocean surface," *Optical Aspects of oceanography*, N.G. Jerlov and E.S. Nielson, Eds., 317-344, Academic Press, San Diego, CA (1974).
22. G.M. Hale, & M.R. Query, "Optical constants of water in the 200-nm to 200- μ m wavelength region," *Appl. Opt.* **12**, 555-563 (1973).
23. R.C. Smith, & K.S. Baker, "Optical properties of the clearest natural waters," *Applied Optics* **20**, 177-184 (1981).
24. A. Bricaud, A. Morel, M. Babin, K. Allali, & H. Claustre, "Variations of light absorption by suspended particles with chlorophyll a concentration in oceanic (case 1) waters: Analysis and implications for bio-optical models," *J. Geophys. Res.* **103**, 31,033-31,044 (1998).
25. R.W. Gould, R.A. Arnone, & P.M. Martinolich, "Spectral dependence of the scattering coefficient in case 1 and case 2 waters," *Appl. Opt.* **38**, 2,377-2,383 (1999).

26. A. Morel, "Optical modeling of the upper ocean in relation to its biogenous matter content (case 1 waters)," *J. of Geophys. Res.* **93**, 10,749-10,768. (1988)
27. H. Loisel, & A. Morel, "Light scattering and chlorophyll concentration in case 1 waters: A reexamination," *Limnol. Oceanogr.* **43**, 847-858 (1998)
28. B.C. Johnson, E. E. Early, R.E. Eplee, Jr., R.A. Barnes, and R. T. Caffrey, "The 1997 Prelaunch Radiometric Calibration of SeaWiFS", Vol. 4 of SeaWiFS Postlaunch Technical Report Series Rep. NASA Tech. Memo. 2000-206892, S.B. Hooker and E.R. Firestone, Eds., NASA Goddard Space Flight Center, Greenbelt, Md, 51 pp., 1999.
29. M. Wang, "A sensitivity study of SeaWiFS atmospheric correction algorithm: Effects of spectral band variations," *Rem. Sens. Environ.* **67**, 348-359 (1999b).
30. Maritorea, S., O'Reilly, J., 2000. Update on the operational SeaWiFS chlorophyll a algorithm. In: *SeaWiFS Postlaunch Calibration and Validation Analyses, Part 2*, SeaWiFS Postlaunch Technical Report Series, NASA Tech. Memo. 1999-206892, Vol. 9, Hooker, S.B., Firestone, E.R. (Eds.), NASA Goddard Space Flight Center, Greenbelt, Maryland. Accepted.
31. C.D. Mobley, "Hydrolight 4.0 Users Guide," Sequoia Scientific, Inc. Mercer Island, WA, 2nd printing, 106 pp. (1998)
32. W.S Pegau, D. Gray & J.R.V. Zaneveld, "Absorption and attenuation of visible and near-infrared light in water: dependence on temperature and salinity," *Appl. Opt.* **36**, 6,035-6,046 (1997).
33. M. Sydor, & R.A. Arnone, "Effect of suspended particulate and dissolved organic matter on remote sensing of coastal and riverine waters," *Appl. Opt.* **36**, 6,905-6,912 (1997).

FIGURE CAPTIONS

Figure 1. The SIMBIOS in situ - SeaWiFS imagery match up comparison for $[\rho_w(\lambda)]_N$ at 412, 443, 490 and *Chl*. The SeaWiFS observations are processed using the standard version 2 processing procedures. Procedures explaining the matchup data set procedure are provided in Ref. 17.

Figure 2. Comparison of $b_{bp}(\lambda)$ and $[\rho_w(\lambda_{NIR})]_N$ estimates versus *Chl* using the SeaBAM data set¹² for a) $b_{bp}(550)$, b) $b_{bp}(865)$, c) $[\rho_w(760)]_N$ and d) $[\rho_w(865)]_N$. The results of the bio-optical algorithm (eq. 6) are shown as the solid line while the points are from the closure model (eq. 7). The dotted horizontal line in c) and d) are estimates of $[\rho_w(\lambda_{NIR})]_N$ assuming that $b_{bp}(\lambda_{NIR})$ equals zero (the clear-water reflectance). The dashed horizontal lines in c) and d) are the one digital count level for the SeaWiFS instrument for bands 7 and 8.²⁸

Figure 3. The errors $[\rho_w(\lambda)]_N$ in the retrieved $[\rho_w(\lambda)]_N$ by ignoring the NIR ocean contributions for the SeaWiFS bands 1-5 for the aerosol M80 model with optical thickness of 0.1 at 865 nm, 7 *Chl* values, and for the solar and viewing geometries of (a) and (c) $\theta_0 = 20^\circ$, $\theta = 20^\circ$, $\phi = 90^\circ$ and (b) and (d) $\theta_0 = 40^\circ$, $\theta = 40^\circ$, $\phi = 90^\circ$. Note that (c) and (d) are in relative errors (%). The curves from the top to the bottom in these figures correspond to *Chl* concentrations of 0.1, 0.3, 0.5, 1.0, 1.5, 2.0, and 5.0 mg m^{-3} , respectively.

Figure 4. SeaWiFS LAC chlorophyll scene for the Chesapeake Bay and adjacent waters from May 19, 1998 (S1998139171559.L1A_HNSG) processed using a) the SeaWiFS standard processing (version 2) and b) the present NIR correction procedure. The purple

dots in a) correspond to the location of field observations used in making figure 5c.

Figure 5. Chlorophyll concentration histograms for observations taken from within Chesapeake Bay from May 19, 1998 using a) the SeaWiFS LAC scene and the standard processing (version 2), b) the SeaWiFS LAC scene with the present NIR correction procedure and c) from in situ observations taken between May 18 and 20, 1998. The purple dots in figure 4a provide the location of the data used in making figure 5c.

Figure 6. The SIMBIOS matchup data set for $[\rho_w(\lambda)]_N$ at 412, 443, 490 and Chl after the NIR correction procedure is performed. The format is identical to figure 1.

Figure 7. Relative error in the SIMBIOS match-up data set for chlorophyll a concentration using a) standard processing and b) with the present NIR bio-optical algorithm. The rms deviation for high chlorophyll conditions ($Chl > 1 \text{ mg m}^{-3}$) decreases by a significant amount after the NIR correction is employed (2.04 to 1.46 mg m^{-3}).

Figure 8. Percentage reduction in SeaWiFS chlorophyll retrievals after implementation of the NIR correction procedure (solid line) as a function of the Chl retrieval from the standard processing. Data are shown for two 8-day composite SeaWiFS GAC scenes for a) summer (Jul 12 - 19, 1998) and b) winter (Jan 17 - 24, 1998) conditions. Also shown is the percentage occurrence of the different Chl intervals (dotted).

Figure 9. Percentage improvement in water-leaving reflectance spectra retrievals (upper) and normalized to the estimated spectra (lower) after implementation of the NIR correction procedure (NIR corrected - standard). Data are shown for two 8-day composite SeaWiFS GAC scenes for summer (right; Jul 12 - 19, 1998) and winter (left; Jan 17 - 24, 1998) conditions. The different lines correspond to categories of Chl concentrations of $10\text{-}20 \text{ mg m}^{-3}$, $5\text{-}10 \text{ mg m}^{-3}$, $2\text{-}5 \text{ mg m}^{-3}$, $1\text{-}2 \text{ mg m}^{-3}$, $0.5\text{-}1 \text{ mg m}^{-3}$, from top to bottom. These results will likely underestimate the NIR error due to assumption that negative

$[\rho_w(\lambda)]_N$ retrievals are zero in the composite making procedure in the present version of SeaWiFS processing.

Table 1: Parameters Used For Determining $[\rho_w(\lambda_{\text{NIR}})]_N$

Center Wavelength	670 nm	760 nm	865 nm	Reference
SeaWiFS Band #	6	7	8	
$a_w(\lambda)$ (m^{-1})	0.4346	2.550	4.286	Ref. 23 for bands 6 & 7 Ref. 22 for band 8
$b_{bw}(\lambda)$ (m^{-1})	0.00041	0.00024	0.00014	Ref. 23
$F_o(\lambda)$ ($\mu\text{W cm}^{-2} \text{nm}^{-1}$)	153.41	122.24	98.82	Ref. 29

Table 2: Ensemble Mean and Standard Deviation (in '()') Estimates for $b_{bp}(550)$, $b_{bp}(760)$ and $b_{bp}(865)$ using SeaBAM (N=919)

Model	$b_{bp}(550)$ (m ⁻¹)	$b_{bp}(760)$ (m ⁻¹)	$b_{bp}(865)$ (m ⁻¹)
Bio-Optical (eq. 6)	0.00322 (0.00358)	0.00250 (0.00290)	0.00227 (0.00268)
Closure (eq. 7)	0.00336 (0.00328)	0.00208 (0.00261)	0.00174 (0.00239)

Table 3: Ensemble Mean and Standard Deviation (in '()') Estimates for $[\rho_w(670)]_N$, **$[\rho_w(760)]_N$ and $[\rho_w(865)]_N$ using SeaBAM (N=919)**

Model	$[\rho_w(670)]_N$ ($\times 10^3$)	$[\rho_w(760)]_N$ ($\times 10^3$)	$[\rho_w(865)]_N$ ($\times 10^3$)
Bio-Optical (eq. 6)	1.085 (0.875)	0.174 (0.184)	0.091 (0.101)
Closure (eq. 7)	1.027 (0.937)	0.148 (0.166)	0.071 (0.091)

TABLE 4. Error $R(i, j)$ (%) in the retrieved ratio of the normalized water-leaving reflectance between the SeaWiFS bands 2 and 5 and bands 3 and 5 for a Maritime RH=80% aerosol model with $\tau_a(865) = 0.1$ and various chlorophyll concentrations and for the two solar and viewing geometries.

<i>Chl</i> (mg/m ³)	$\theta_0=20^\circ, \theta=20^\circ, \Delta\phi=90^\circ$		$\theta_0=40^\circ, \theta=40^\circ, \Delta\phi=90^\circ$	
	R_{25} (%)	R_{35} (%)	R_{25} (%)	R_{35} (%)
0.1	1.13	1.02	2.05	1.89
0.3	0.96	1.43	0.90	1.83
0.5	-0.51	1.17	-1.55	1.21
1.0	-6.49	-0.58	-9.98	-1.37
1.5	-13.56	-3.00	-18.02	-4.19
2.0	-20.22	-5.45	-25.63	-7.05
5.0	-66.27	-23.56	-60.48	-21.63

TABLE 5. Error in the retrieved chlorophyll concentration using the Morel-3 and OC2v2 algorithms. The atmosphere is specified as a Maritime RH=80% aerosol type with $\tau_a(865) = 0.1$. Various true chlorophyll concentrations are used for two solar and viewing geometries.

<i>Chl</i> (mg/m ³)	$\theta_o=20^\circ, \theta=20^\circ, \Delta\phi=90^\circ$		$\theta_o=40^\circ, \theta=40^\circ, \Delta\phi=90^\circ$	
	Morel-3 (%)	OC2v2 (%)	Morel-3 (%)	OC2v2 (%)
0.1	-2.0	-2.8	-3.7	-5.1
0.3	-1.5	-3.3	-1.4	-4.2
0.5	0.8	-2.7	2.6	-2.7
1.0	12.0	1.3	18.4	3.15
1.5	26.9	7.0	35.8	9.8
2.0	42.2	12.9	53.4	16.7
5.0	158.2	58.2	144.4	53.4

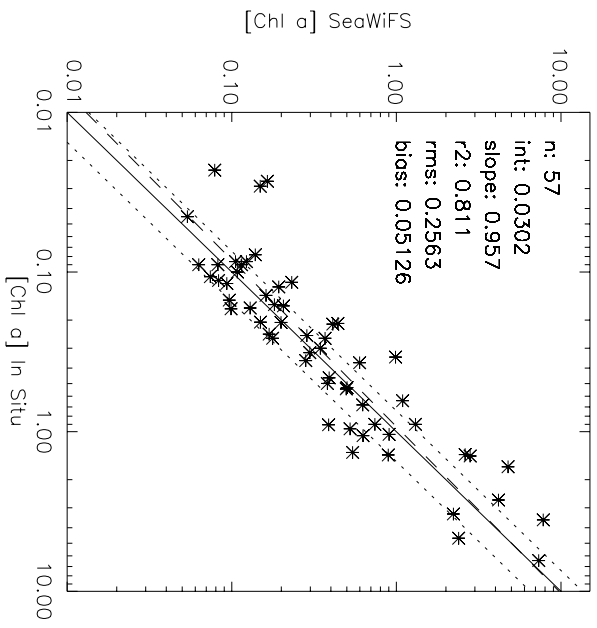
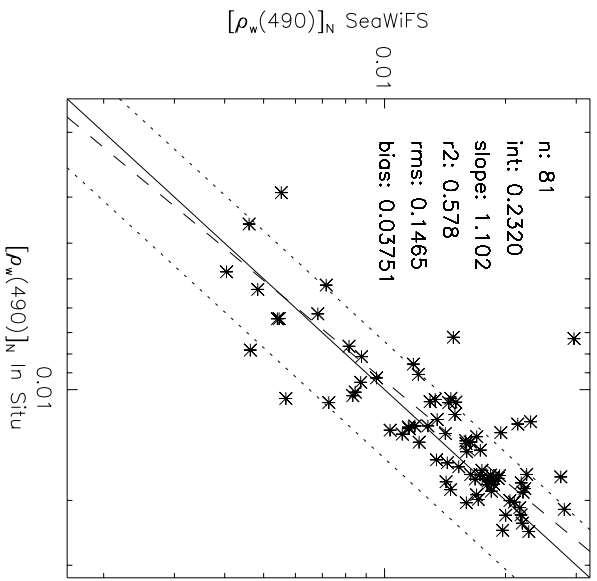
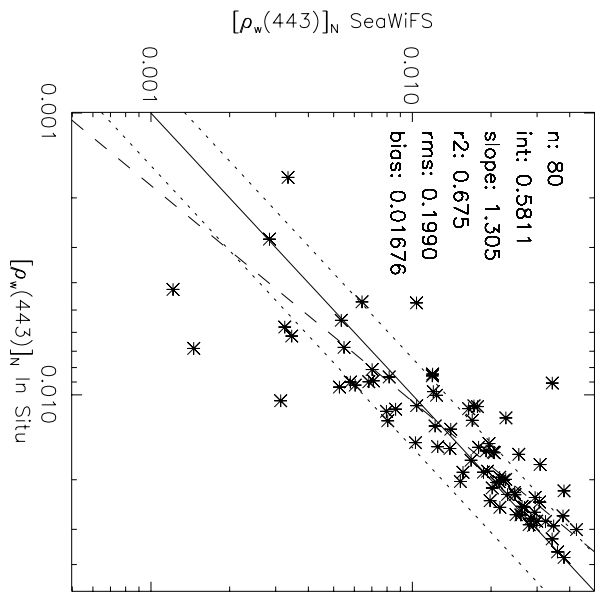
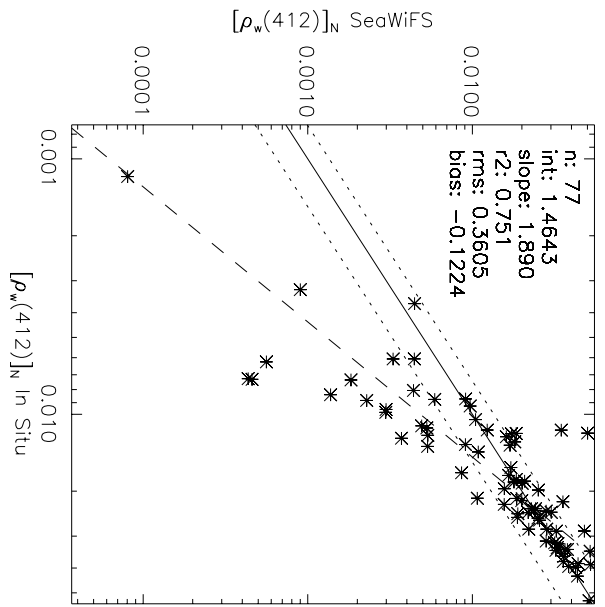


Figure 2.

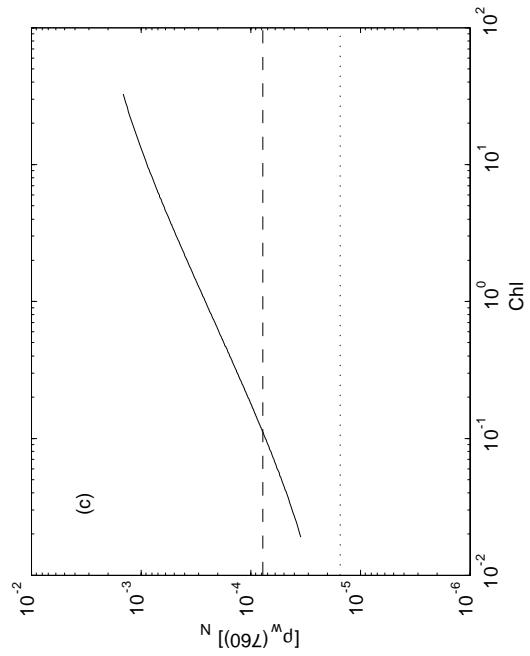
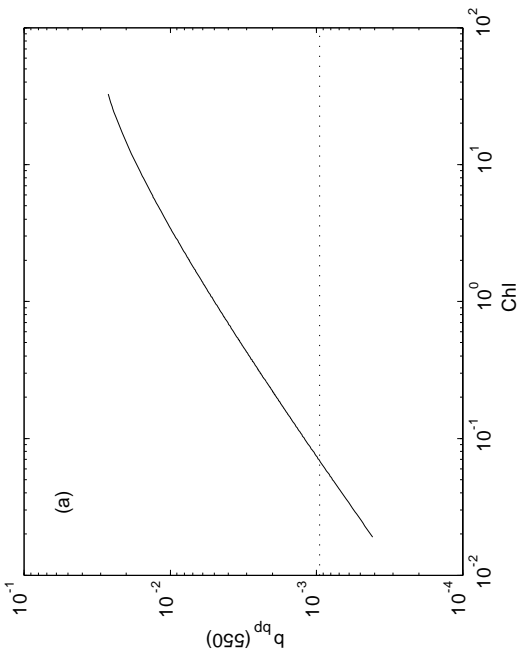
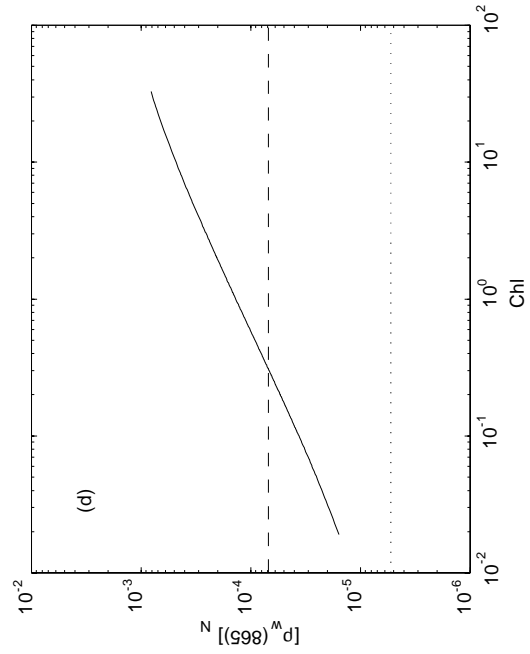
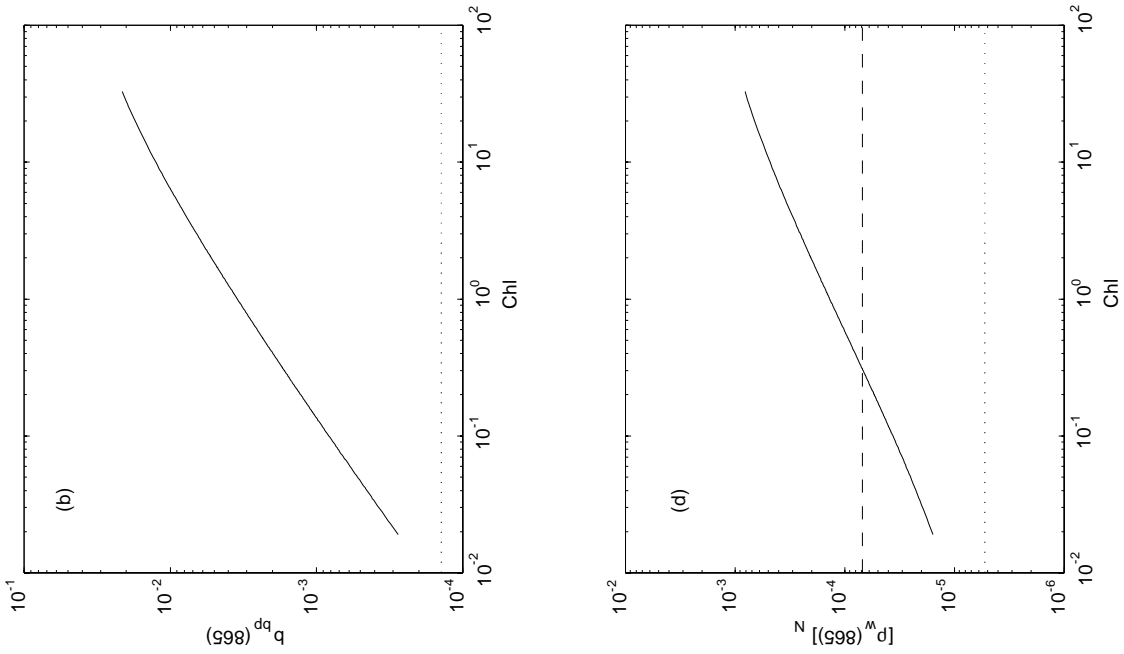


Figure 3.

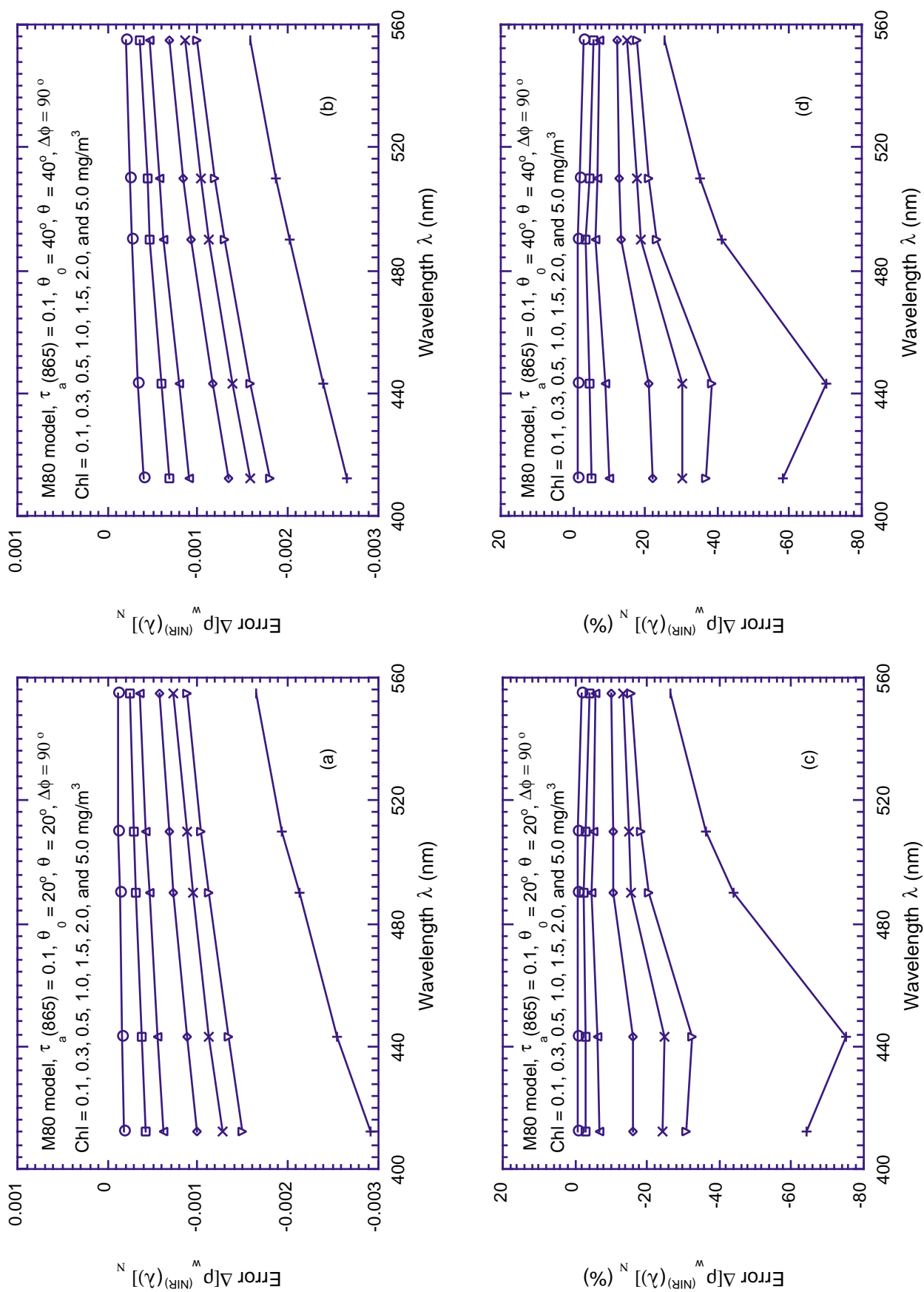


Figure 4.

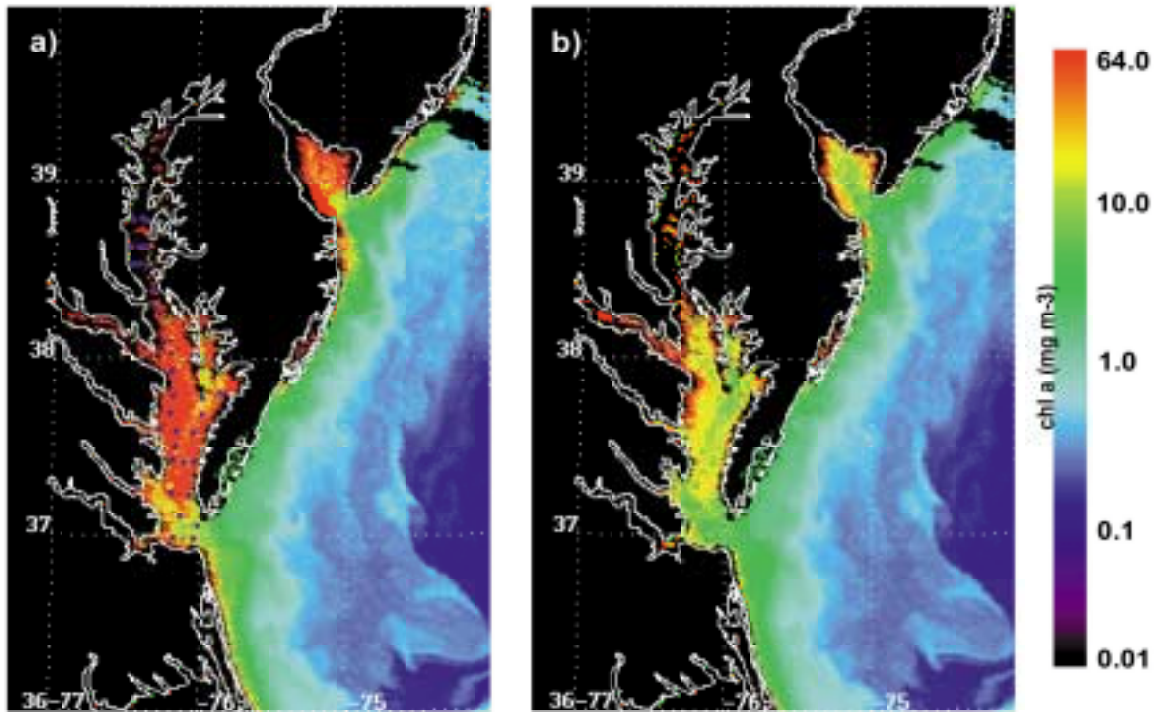
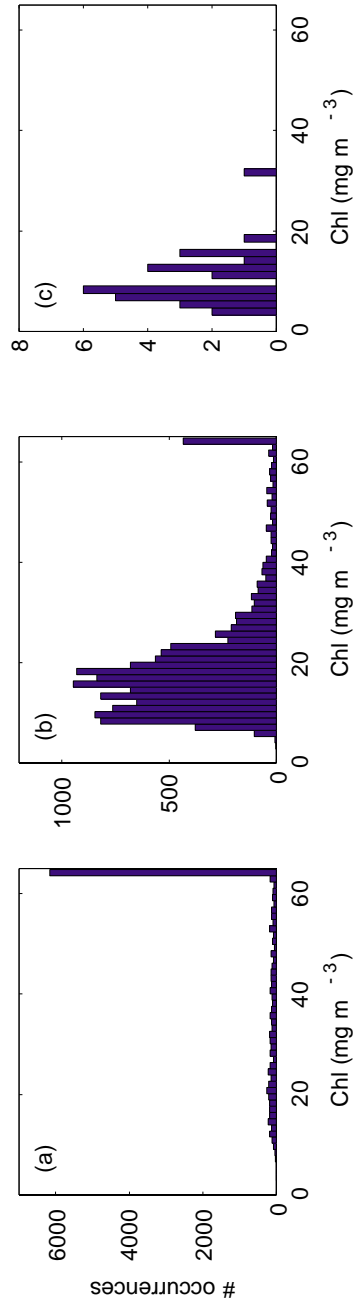


Figure 5.



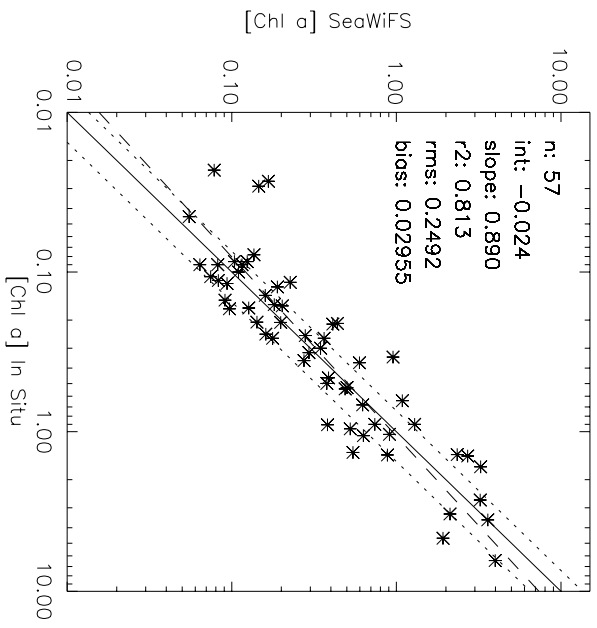
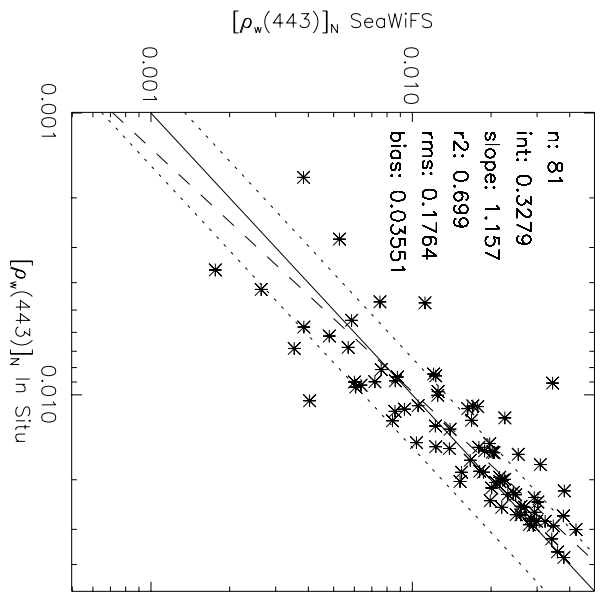
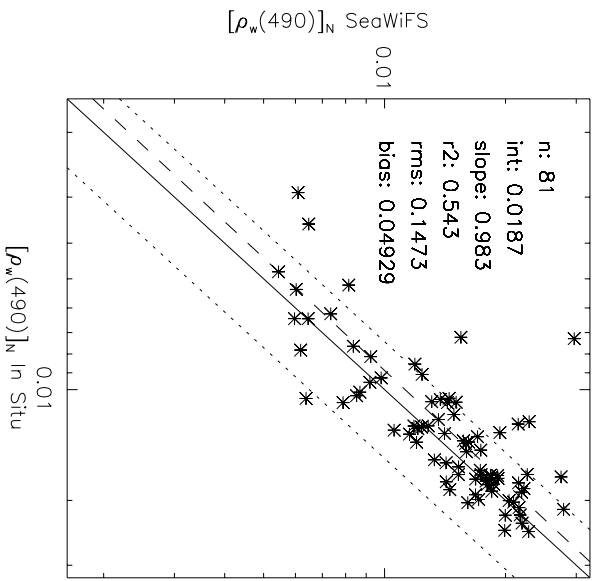
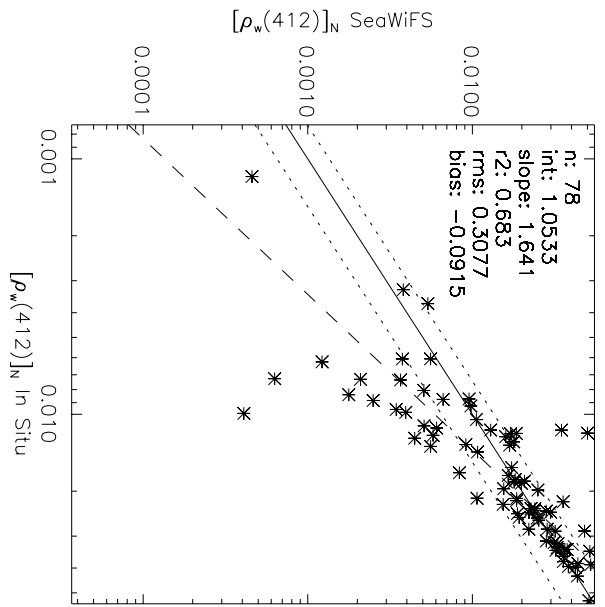


Figure 7.

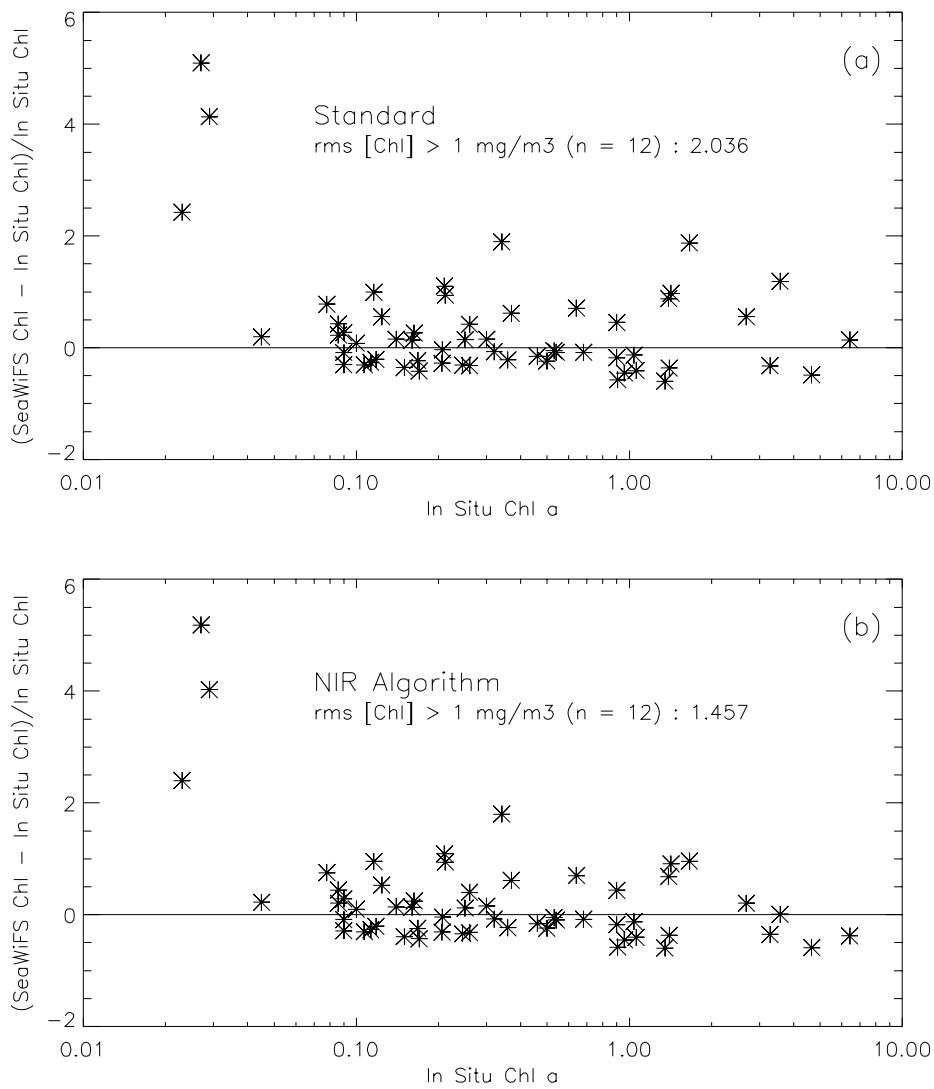


Figure 8.

